Electronic Supplementary Information for article:

OH-stretch overtone of methanol: empirical assignment using two temperature technique in supersonic jet

Vít Svoboda,[a,b] Veronika Horká-Zelenková,[a] Jozef Rakovský,[a] Petr Pracna, [a] and Ondrej Votava [a,*]

a) J. Heyrovský Institute of Physical Chemistry, Dolejškova 2155/3, 182 23 Prague 8, Czech Republic
b) Institute of Chemical Technology Prague, Department of Physical Chemistry, Technická 5, 166 28 Prague 6, Czech Republic.

*Correspondence and proofs to:
Mgr. Votava Ondrej, Ph. D.
Molecular and Cluster Dynamics Group
Dolejškova 2155/3, 182 23 Prague 8, Czech Republic
Email: ondrej.votava@jh-inst.cas.cz
Phone: +420 26605 3636

Two temperature analysis – derivation of equations

The two temperature analysis utilizes the temperature dependence of spectral line intensities to aid lower state rotational assignments. Integrated line strength $S(T)$ are proportional to the lower state populations and at thermal equilibrium those are determined by the Boltzmann distribution. Therefore:

$$S(T) \propto \frac{\exp\left[\frac{-E''}{\mathbf{k}_B \cdot T}\right]}{Q(T)}, \tag{1}$$

where E'' is lower state rotational energy in the vibrational ground state and $Q(T)$ is the partition function at particular temperature. The fact that methanol exists in a form of two nuclear spin isomers must be considered in the evaluation of partition functions at very low temperatures in the supersonic expansions. In the case of thermal equilibrium at temperatures approaching 0 K only the lowest state of ortho isomer of CH_3OH would be populated. However, under the conditions of rapid cooling in the supersonic molecular beam the nuclear spin conversion is highly inefficient and nuclear spin isomers maintain their concentration ratios of the high temperature limit. Methanol cooling in the supersonic expansion must be considered as non-equilibrium process where each nuclear spin isomer behaves as an independent specie with partition functions given by:

$$Q_{ortho} = \sum_{ortho} g_{T,o} \cdot g_{I,o} \cdot (2J+1) \cdot e^{\frac{-E''}{\mathbf{k}_B T}}, \tag{2}$$

$$Q_{para} = \sum_{para} g_{T,p} \cdot g_{I,p} \cdot (2J+1) \cdot e^{\frac{-E''}{\mathbf{k}_B T}}. \tag{3}$$

Nuclear spin statistical weight factor g_I for ortho nuclear spin isomer is $g_{I,o} = 4$ and for para nuclear spin isomer is $g_{I,p} = 2$. Ortho states belong to A irreducible species of torsional symmetry group, therefore $g_{T,o} = 1$. Para states belong to E species, which is doubly degenerate, but because all levels with $K \neq 0$ are split into two state their factor is $g_{T,p} = 1$, only levels with $K = 0$ have factor $g_{T,p} = 2$ [for more detail, see R. M. Lees, *The Astronomical Journal*, **184**, 763-771 (1973)]. Summations in partition function are taken over all states of a given isomer. For convenience, methanol rotational energies used for partition function evaluation for states up to $J'' = 20$ are included in separate plain text file ESIrotenergies.txt.

The ratio of line intensities at two different temperatures T_1 and T_2 respectively, is given by:

$$R_{th}(T_1, T_2) \equiv \frac{S(T_1)}{S(T_2)} = \frac{Q(T_2)}{Q(T_1)} e^{\frac{-E''}{\mathbf{k}_B}\left(\frac{1}{T_1} - \frac{1}{T_2}\right)} \quad . \tag{4}$$

This quantity is independent on the line strength parameters of given spectral line and also on degeneracy factors which are independent on J. When the ground state rotational energies are known, ratios can be calculated.

In absorption measurement the integrated line strength $S(T)$ and the experimental integrated absorbance $\Sigma(T)$ are related via the Lambert – Beer law which can be written in form:

$$\Sigma(T) \equiv \int_{line} ln\left(\frac{I_0}{I}\right) \mathrm{d}\nu = S(T) \cdot N_u, \tag{5}$$

where the integrated column density N_u is defined as:

$$N_u \equiv \int_0^l N_0(x) \mathrm{d}x, \tag{6}$$

where N_0 is the number density of absorbing molecules and l is the absorption path length. Therefore the ratio of the experimental integrated absorbances for given transition is related to the line strength ratio $R_{exp}(T_1, T_2)$ via equation:

$$\frac{\Sigma(T_1)}{\Sigma(T_2)} = f(T_1, T_2) \cdot R_{exp}(T_1, T_2), \tag{7}$$

where

$$f(T_1, T_2) \equiv \frac{N_u(T_1)}{N_u(T_2)}. \tag{8}$$

Scaling factor $f(T_1, T_2)$ depends on the experimental conditions and has the same value for all spectral lines. In a specific case when the molecular number density and the absorption path length are equal for spectra measured at T_1 and T_2 the scaling factor $f(T_1, T_2) = 1$ and thus the experimental intensity ratio $R_{exp}(T_1, T_2)$ is equal to the measured ratio of integrated absorbances. This is often the case for static cell experiments. However in supersonic jet expansions the total pressure and mixing ratio varies widely for spectra measured at different temperatures and

thus the value of scaling factor $f(T_1, T_2)$ must be determined experimentally to match the experimental intensity ratios with the predicted values R_{th}.

Experimental apparatus

Experimental setup used for all measurements in this work has been designed at the J. Heyrovský institute in Prague. The apparatus combines a pulsed slit-jet supersonic nozzle with a tunable diode laser direct-absorption spectrometer.

The laser spectrometer consists of tunable extended cavity diode laser (ECDL) in Littmann configuration with an anti-reflection coated laser diode. Laser is tunable in a wide range of 7070 – 7300 cm^{-1}. The laser is coarse-tuned using motorized precision screw and fine-tuned by piezoelectric transducer (PZT) enabling continuous frequency scans over 6 cm^{-1}. The laser tuning system is controlled by a master PC and allows automatic tuning over the full range comprising of many partially overlapped single PZT scans.

Wavemeter and temperature stabilized Fabry–Pérot etalon enable frequency calibration of spectra. The light is detected using autoballanced differential photodetection unit. The unit provides two outputs signals: the differential signal ΔI, proportional to the difference between the light intensity on the signal and reference photodiode (for detail see text), and I_0, the signal proportional to the total light intensity on the signal detector only.

The supersonic expansion is produced by a slit nozzle (40×0.1 mm^2) with solenoid actuated pulsed valve producing short ($\Delta t \leq 1$ ms), high intensity gas pulses typically at 3 Hz repetition rates.

New gas inlet system (2014) has been used for precise control of the gas mixture composition that consists of methanol vapor in rare gas RG (helium or argon) buffer gas. The inlet system has two parallel input lines. The first input is filled by the RG mixed with saturated methanol vapor evaporated from liquid metanol reservoir at room temperature. This pre-mixture input is further diluted with pure RG from the second line to form final mixture. Both flows are adjusted by mass flow controller FC. This system allows control of mixing ratio and total stagnation pressure before the nozzle which leads to changes in resulting methanol concentration in the expansion.

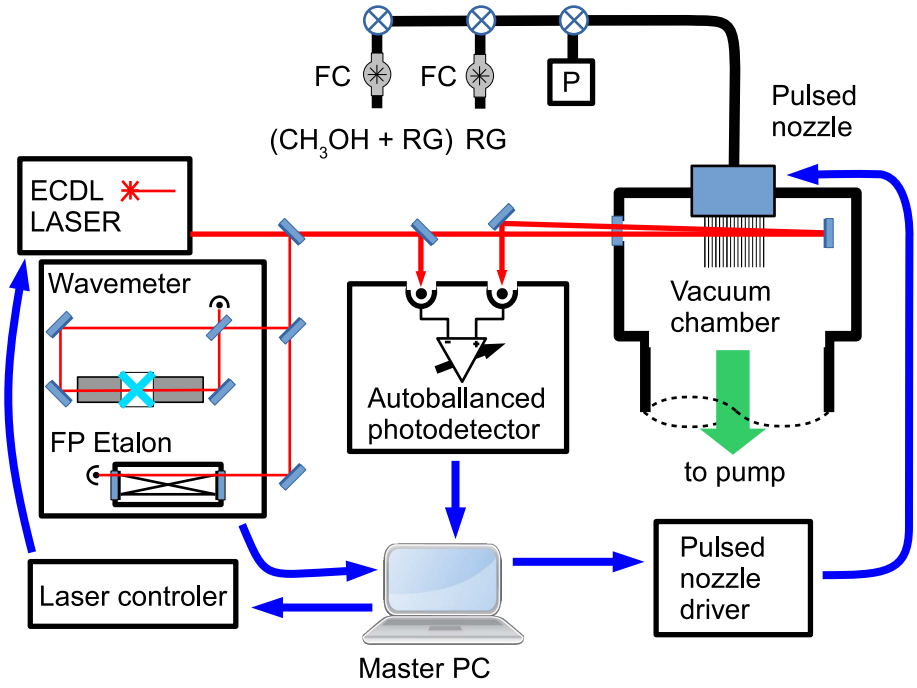

Characterization of methanol expansion

The two temperature analysis requires measurement of the spectra at two different and well defined temperatures. Because the temperature established in the jet expansion is strongly influenced by experimental conditions, especially by pressure and composition of expanding gas, we must characterize these conditions in a detail. The local kinetic temperature of the molecular beam is determined from Doppler broadening of the spectral lines. Since it has been demonstrated that equilibrium is well established between the kinetic and rotational temperatures in the planar expansions, Doppler broadening measurements represent a good approximation to the methanol rotational temperature in the expansion. Relative concentrations and local temperatures in the molecular beam were determined from integrated absorbance and Doppler line widths of selected strong and well isolated spectral line at 7195.9189 cm^{-1}. Figure shows plots where the results are compared for CH_3OH co-expansion with two different buffer gases – Ar or He.

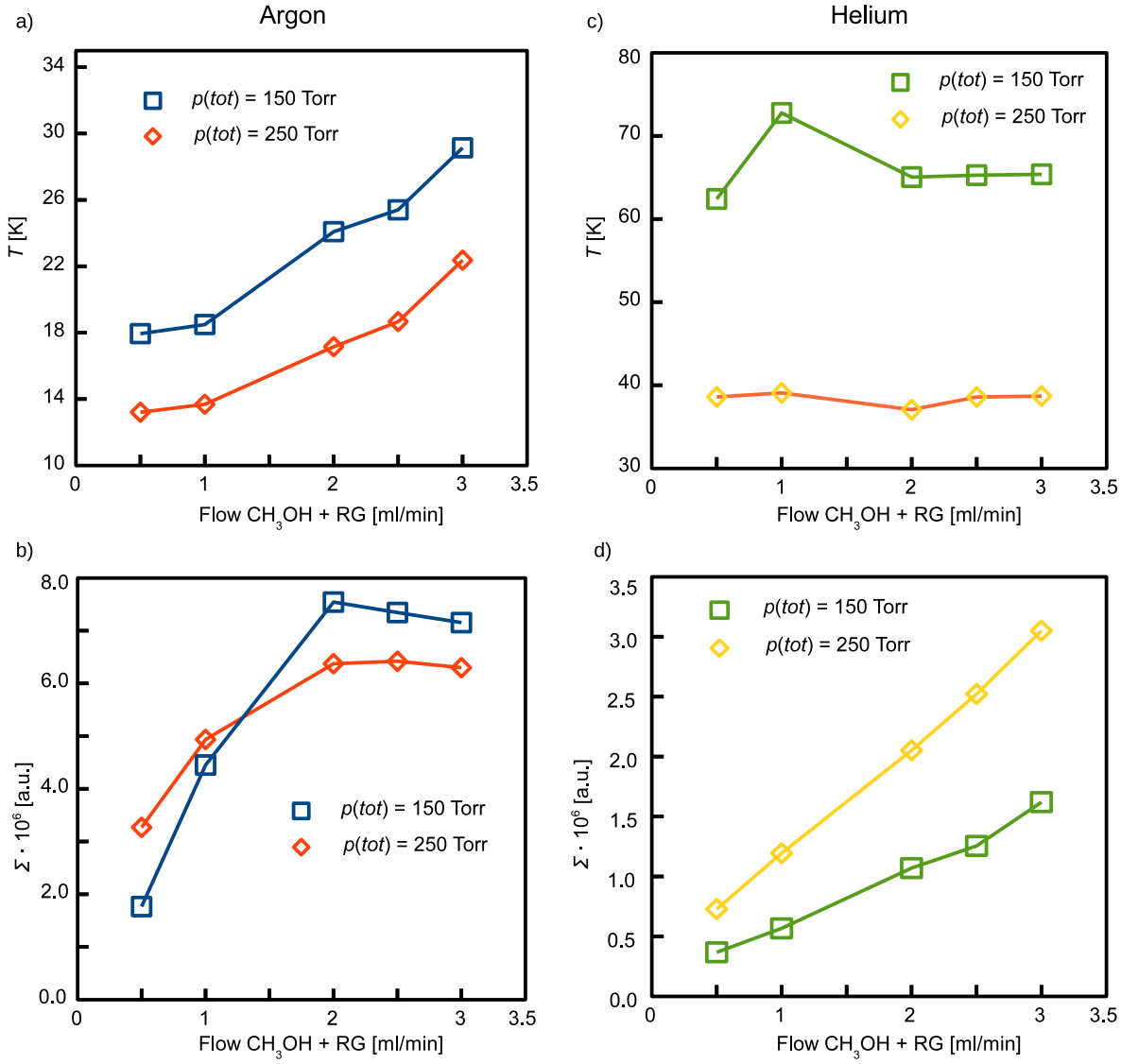

Plots a) and c) from figure show the measurement of the temperature in co-expansion with Ar or He in dependence on the flow rate of the pre-mixture CH_3OH + rare gas (RG) for different stagnation pressures in front of the nozzle. The results are discussed as follows: i) expansion with Ar produces lower temperatures than He expansion and ii) expansion temperature decreases with increasing stagnation pressure for both rare gasses. Major difference between Ar and He expansion is that increasing CH_3OH concentration (flow rate of the pre-mixture) does not change temperature significantly for He expansion but the temperature increases in Ar expansion.

This is most likely caused by cluster formation at higher CH_3OH concentrations. This cluster formation consequently affects the temperature of the expansion due to release of condensation heat (see plot a)). On the other hand, cluster formation is negligible in the case of He expansion because He has lower polarizability than Ar. The fact that in Ar expansion clustering occurs consequently leads to decrease of the monomer intensity at higher CH_3OH concentration, *i.e.* higher flow rate of the pre-mixture (see plot b) and d)). On the other hand, Ar expansion produces colder expansions at low methanol concentrations.

In summary, we have demonstrated that the beam temperature can be changed over a wide range between 13 and 100 K by controlling the CH_3OH mixing ratio and stagnation pressure before the nozzle and also by choosing the proper buffer gas. As the primary goal of this study is to determine rotational assignments for spectral lines originating from the lowest rotational energy levels, eliminating higher rotational states by reducing expansion temperature to lowest possible values has been desirable.

High resolution spectra of OH-stretch overtone

Three spectra measured at different temperatures - 13, 23, and 56 K. Figure shows that with decreasing temperature the number of lines is reduced and also the profile of the band is changing. Several gaps in the 13 K spectrum are caused by laser mode-hopes and ranges where the laser exhibited multimode behavior. Such regions have been separately re-scanned at different laser driving current and/or temperature to cover the gaps.

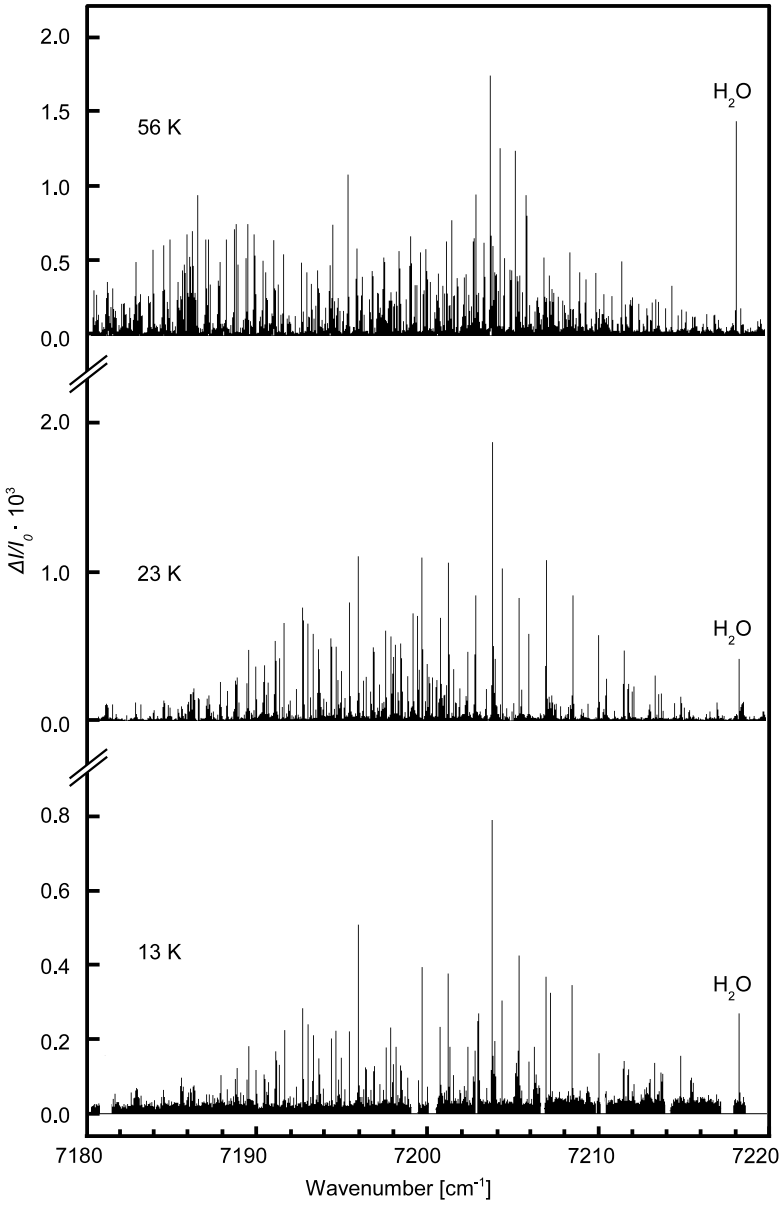

Subset of 37 high intensity lines with possible assignments based on TTA analysis

The complete data set (37 lines) used to demonstrate the TTA procedure for methanol based on $R_{exp}(13,56)$. All included transitions have $\Sigma_{13\mathrm{K}} > 4.04 \cdot 10^{-7}$ cm^{-1}. Transitions are sorted by decreasing value $R_{exp}(13,56)$. First 21 transitions are consistent only with one of the four lowest states $(0,0,A)$, $(1,0,A)$, $(2,0,A)$, and $(1,-1,E)$, respectively, and were subject to further analysis using GSCD. Remaining 16 transitions can be also assigned to higher states and were not systematically checked by GSCD at this point.

position/cm^{-1}	Σ_{13K}/cm^{-1}	$R(13,56)$	Probable lower state
7206.9078	1.189E-06	12.17	(0,0,A), (1,0,A)
7205.3378	1.220E-06	11.42	(0,0,A), (1,0,A)
7196.3742	4.064E-07	10.25	(0,0,A), (1,0,A), (1,-1,E)
7198.1151	6.236E-07	9.26	(0,0,A), (1,0,A), (1,-1,E), (2,0,A)
7208.4607	1.107E-06	9.21	(1,0,A), (1,-1,E), (2,0,A)
7197.8219	7.028E-07	9.11	(1,0,A), (1,-1,E), (2,0,A)
7195.9195	1.407E-06	9.11	(1,0,A), (1,-1,E), (2,0,A)
7194.9242	4.846E-07	8.68	(1,0,A), (1,-1,E), (2,0,A)
7194.6216	7.246E-07	8.53	(1,0,A), (1,-1,E), (2,0,A)
7209.9897	5.074E-07	7.98	(1,-1,E), (2,0,A), (2,-1,E)
7193.2745	7.285E-07	7.78	(1,-1,E), (2,0,A), (2,-1,E), (0,0,E)
7200.7218	7.812E-07	7.72	(1,-1,E), (2,0,A), (2,-1,E), (0,0,E)
7199.6677	1.279E-06	7.67	(1,-1,E), (2,0,A), (2,-1,E), (0,0,E)
7201.2638	5.451E-07	7.63	(1,-1,E), (2,0,A), (2,-1,E), (0,0,E)
7202.3472	4.749E-07	7.56	(1,-1,E), (2,0,A), (2,-1,E), (0,0,E)
7201.2051	1.298E-06	7.51	(1,-1,E), (2,0,A), (2,-1,E), (0,0,E)
7192.6928	9.840E-07	7.46	(1,-1,E), (2,0,A), (2,-1,E), (0,0,E)
7202.3270	6.577E-07	7.37	(1,-1,E), (2,0,A), (2,-1,E), (0,0,E)
7192.9815	8.154E-07	7.29	(1,-1,E), (2,0,A), (2,-1,E), (0,0,E)
7197.9782	4.851E-07	6.64	(2,0,A), (2,-1,E), (0,0,E), (1,0,E)
7195.9416	6.294E-07	6.59	(2,0,A), (2,-1,E), (0,0,E), (1,0,E)
7203.7831	5.825E-07	5.79	(2,-1,E), (0,0,E), (1,0,E), (3,0,A)
7191.1284	4.590E-07	5.62	(0,0,E), (1,0,E), (3,0,A), (3,-1,E)
7203.8112	4.244E-07	5.61	(0,0,E), (1,0,E), (3,0,A), (3,-1,E)
7194.3463	6.570E-07	5.55	(0,0,E), (1,0,E), (3,0,A), (3,-1,E)
7191.6008	7.525E-07	5.41	(0,0,E), (1,0,E), (3,0,A), (3,-1,E)
7191.3040	4.620E-07	5.39	(0,0,E), (1,0,E), (3,0,A), (3,-1,E)
7202.7543	4.660E-07	5.24	(1,0,E), (3,0,A), (3,-1,E)
7189.5056	5.864E-07	5.15	(1,0,E), (3,0,A), (3,-1,E), (2,0,E)
7197.5350	5.995E-07	4.85	(1,0,E), (3,0,A), (3,-1,E), (2,0,E), (1,1,A+), (1,1,A-)
7204.3371	1.073E-06	4.74	(1,0,E), (3,0,A), (3,-1,E), (2,0,E), (1,1,A+), (1,1,A-)
7196.8715	4.303E-07	4.60	(3,0,A), (3,-1,E), (2,0,E), (1,1,A+), (1,1,A-), (1,1,E)
7193.6060	5.077E-07	4.47	(3,0,A), (3,-1,E), (2,0,E), (1,1,A+), (1,1,A-), (1,1,E)
7191.0677	5.910E-07	4.25	(3,0,A), (3,-1,E), (2,0,E), (1,1,A+), (1,1,A-), (1,1,E)
7205.8917	4.509E-07	3.59	(1,1,A-), (1,1,E), (2,1,A+), (2,1,A-), (4,0,A)
7198.3971	4.826E-07	3.48	(1,1,A-), (1,1,E), (2,1,A+), (2,1,A-), (4,0,A)
7195.4059	7.204E-07	3.46	(1,1,A-), (1,1,E), (2,1,A+), (2,1,A-), (4,0,A)

Schematic diagram for ground state combination differences

Ground state combination differences for state $(0, 0, A)$. Transitions originating from this state are in solid lines (1 and 2 respectively) while corresponding transitions sharing the upper state are in dashed lines. Resulting GSCDs are highlighted by red arrows. Dashed dotted line highlights unique GSCD distinguishing transition 1 from transition 2.

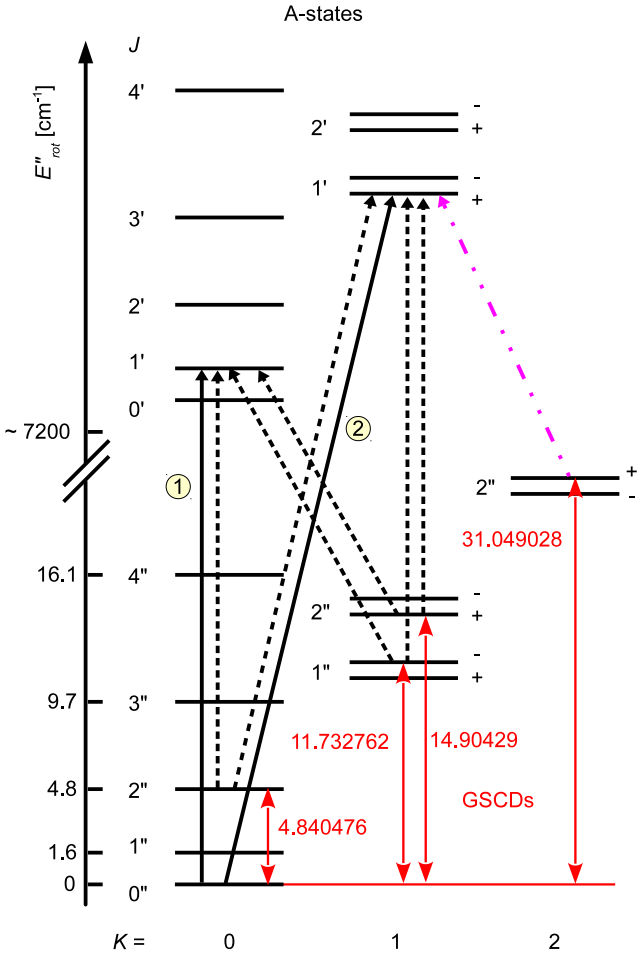

Complete list of GSCD confirmed assignments

List of all combination differences (last three columns) for the 15 lines with assignments confirmed by GSCD from table 2 of the paper (first three columns).

			GSCDs		
position/cm^{-1}	Lower state	Assignment	position/cm^{-1}	Lower state	Calc. − Meas./cm^{-1}
7197.8219	(0,0,A)	$^{q}R0$	7192.9809	(2,0,A+)	0.00052
			7186.0887	(1,1,A-)	0.00041
			7182.9168	(2,1,A+)	0.00078
7198.1151	(0,0,A)	$^{q}R0$	7193.2741	(2,0,A+)	0.00044
			7186.3815	(1,1,A-)	0.00081
			7183.2100	(2,1,A+)	0.00077
7205.3378	(0,0,A)	$^{r}R0$	7200.4973	(2,0,A+)	0.00002
			7193.6051	(1,1,A-)	-0.00002
			7190.4336	(2,1,A+)	-0.00009
			7174.2889	(2,2,A+)	-0.00010
7194.6216	(1,0,A)	$^{q}P1$	7184.5295	(1,1,A+)	0.00076
7194.9242	(1,0,A)	$^{q}P1$	7184.8322	(1,1,A+)	0.00062
7199.6677	(1,0,A)	$^{q}R1$	7191.5998	(3,0,A+)	0.00085
			7186.2929	(2,1,A-)	0.00064
			7189.5757	(1,1,A+)	0.00067
			7181.5774	(3,1,A+)	0.00072
7206.9078	(1,0,A)	$^{r}R1$	7198.8404	(3,0,A+)	0.00028
			7193.5332	(2,1,A-)	0.00035
			7196.8161	(1,1,A+)	0.00027
			7188.8178	(3,1,A+)	0.00038
			7172.6309	(3,2,A+)	0.00027
			7177.4723	(2,2,A-)	0.00005
7192.9815	(2,0,A)	$^{q}P2$	7182.9170	(2,1,A+)	0.00068
			7186.0886	(1,1,A-)	0.00055
			7197.8219	(0,0,A+)	0.00007
7193.2745	(2,0,A)	$^{q}P2$	7183.2102	(2,1,A+)	0.00055
			7186.3819	(1,1,A-)	0.00032
			7198.1151	(0,0,A+)	-0.00003
7201.2051	(2,0,A)	$^{q}R2$	7191.1411	(2,1,A+)	0.00022
			7186.1754	(3,1,A-)	0.00010
			7189.9120	(4,0,A+)	0.00008
			7179.9443	(4,1,A+)	0.00005
7201.2638	(2,0,A)	$^{q}R2$	7191.1997	(2,1,A+)	0.00023
			7186.2334	(3,1,A-)	0.00077
			7189.9702	(4,0,A+)	0.00048
			7180.0025	(4,1,A+)	0.00052
7208.4607	(2,0,A)	$^{r}R2$	7198.3968	(2,1,A+)	0.00009
			7193.4309	(3,1,A-)	0.00013
			7177.4114	(3,2,A-)	-0.00001
			7197.1677	(4,0,A+)	-0.00006
			7187.1997	(4,1,A+)	0.00015
			7170.9560	(4,2,A+)	0.00014
7196.3742	(1,-1,E)		7193.1475	(2,-1,E)	-0.00014
			7191.1280	(1,0,E)	0.00024
			7185.6224	(1,1,E)	0.00031
			7177.5550	(3,1,E)	-0.00080
7197.9782	(1,-1,E)	$^{r}Q1$	7189.9120	(3,-1,E)	-0.00064
			7194.7513	(2,-1,E)	-0.00001
			7187.2265	(1,1,E)	0.00024
			7194.3459	(0,0,E)	-0.00001
			7189.5051	(2,0,E)	0.00007
			7183.9993	(2,1,E)	-0.00003
7202.3270	(1,-1,E)	$^{r}P1$	7197.0810	(1,0,E)	-0.00003

Spectral lines with measured intensity ratios

The table provides all 147 lines measured both in 13 and 56 K spectra for which intensity ratio R_{exp} was measured. The table is also provided as a separate plain text data file ESIlines.txt.

position/cm^{-1}	$\Sigma(13K)$/cm^{-1}	$R_{exp}(13,56)$	position/cm^{-1}	$\Sigma(13K)$/cm^{-1}	$R_{exp}(13,56)$
7187.8102	1.012E-07	2.30	7197.1682	2.165E-07	4.47
7187.8298	7.273E-08	2.24	7197.3216	1.099E-07	3.27
7187.8749	3.102E-07	3.78	7197.4033	1.187E-07	4.30
7187.8896	1.254E-07	4.66	7197.5350	5.995E-07	4.85
7188.2365	1.483E-07	3.45	7197.5596	1.590E-07	4.98
7188.2747	2.132E-07	2.74	7197.8219	7.028E-07	9.11
7188.6188	9.667E-08	4.55	7197.8989	1.505E-07	3.68
7188.6960	9.432E-08	3.78	7197.9412	2.278E-07	3.70
7188.7341	3.227E-07	3.12	7197.9782	4.851E-07	6.64
7188.8187	3.622E-07	3.41	7198.1151	6.236E-07	9.26
7188.9511	8.917E-08	1.74	7198.2296	1.418E-07	2.84
7189.4296	2.609E-07	3.97	7198.3971	4.826E-07	3.48
7189.4875	8.330E-08	3.98	7198.4587	3.783E-07	3.61
7189.5056	5.864E-07	5.15	7198.5044	1.893E-07	3.72
7189.5772	9.719E-08	5.82	7198.8407	2.926E-07	4.88
7190.3587	8.927E-08	3.60	7199.6677	1.279E-06	7.67
7190.3905	2.317E-07	3.53	7199.9677	2.263E-07	2.22
7190.4342	3.612E-07	3.65	7200.6299	1.389E-07	4.33
7190.5648	1.666E-07	2.63	7200.6577	1.751E-07	6.76
7190.6301	8.977E-08	3.41	7200.6967	1.315E-07	5.08
7190.6349	1.586E-07	3.75	7200.7076	1.332E-07	3.63
7190.6615	1.477E-07	3.96	7200.7218	7.812E-07	7.72
7190.6738	2.843E-07	5.58	7200.7315	1.573E-07	8.01
7191.0387	2.130E-07	5.09	7200.7577	9.706E-08	3.99
7191.0574	8.600E-08	1.56	7200.7799	2.707E-07	7.37
7191.0677	5.910E-07	4.25	7200.8343	1.645E-07	7.24
7191.0792	9.251E-08	1.92	7200.8616	1.327E-07	10.51
7191.0948	1.547E-07	3.59	7200.9622	1.759E-07	3.98
7191.1284	4.590E-07	5.62	7201.0069	9.896E-08	5.70
7191.1423	9.489E-08	3.49	7201.0785	2.111E-07	3.72
7191.3040	4.620E-07	5.39	7201.1876	1.188E-07	10.45
7191.4883	1.258E-07	4.41	7201.2051	1.298E-06	7.51
7191.6008	7.525E-07	5.41	7201.2638	5.451E-07	7.63
7191.8470	1.075E-07	3.71	7201.3937	6.913E-08	4.14
7191.9240	1.375E-07	4.35	7201.5213	3.084E-07	3.05
7192.2875	2.513E-07	6.71	7201.6176	1.201E-07	3.14
7192.5630	7.754E-08	8.38	7201.6432	1.025E-07	2.66
7192.6928	9.840E-07	7.46	7201.8448	2.110E-07	3.37
7192.7704	9.479E-08	3.15	7202.1621	1.544E-07	6.60
7192.9815	8.154E-07	7.29	7202.2403	2.248E-07	7.33
7193.1215	1.398E-07	4.57	7202.2621	1.082E-07	2.47
7193.1362	6.934E-08	6.19	7202.3126	7.789E-08	4.75
7193.2745	7.285E-07	7.78	7202.3270	6.577E-07	7.37
7193.4318	1.226E-07	6.64	7202.3472	4.749E-07	7.56
7193.5340	1.680E-07	4.59	7202.4407	1.224E-07	9.90
7193.6060	5.077E-07	4.47	7202.4873	8.831E-08	7.97
7193.6412	1.130E-07	3.76	7202.6762	2.034E-07	6.30
7193.6735	3.424E-07	4.25	7202.7543	4.660E-07	5.24
7193.6999	1.848E-07	3.96	7203.4202	1.949E-07	3.29
7193.8886	1.890E-07	6.75	7203.7322	3.846E-07	7.57
7194.3463	6.570E-07	5.55	7203.7831	5.825E-07	5.79
7194.3701	1.270E-07	2.66	7203.8112	4.244E-07	5.61
7194.3929	1.083E-07	2.72	7204.2524	8.735E-08	2.20
7194.6216	7.246E-07	8.53	7204.3371	1.073E-06	4.74
7194.7517	3.099E-07	6.08	7204.3509	1.712E-07	13.55
7194.9242	4.846E-07	8.68	7205.3378	1.220E-06	11.42
7195.1108	1.085E-07	4.89	7205.4804	1.619E-07	2.86
7195.1247	1.745E-07	4.63	7205.8917	4.509E-07	3.59

Continued on next page

Continued from previous page

7195.4059	7.204E-07	3.46	7206.9078	1.189E-06	12.17
7195.4744	1.157E-07	2.27	7206.9853	1.256E-07	5.53
7195.8793	1.088E-07	3.55	7208.2099	1.287E-07	8.76
7195.8969	1.044E-07	2.06	7208.3463	8.903E-08	4.57
7195.9077	3.198E-07	8.29	7208.3644	9.705E-08	8.09
7195.9195	1.407E-06	9.11	7208.4403	1.976E-07	6.02
7195.9416	6.294E-07	6.59	7208.4607	1.107E-06	9.21
7195.9563	2.048E-07	7.04	7208.4689	1.567E-07	7.12
7195.9926	9.457E-08	3.64	7208.5171	1.381E-07	6.99
7196.2376	1.971E-07	2.83	7209.9897	5.074E-07	7.98
7196.3742	4.064E-07	10.25	7210.0053	1.331E-07	8.72
7196.6558	1.735E-07	3.57	7212.9502	1.102E-07	12.90
7196.7177	9.018E-08	3.17	7213.2803	3.662E-07	11.85
7196.8168	4.010E-07	4.02	7213.5026	1.244E-07	4.99
7196.8715	4.303E-07	4.60	7216.9010	1.029E-07	7.73
7216.9196	9.656E-08	8.50			